Intermolecular Interactions of Trichloromethyl Group in the Crystal State, the Case of 2-Trichloromethyl-3H-4-quinazoline Polymorphs and 1-Methyl-2-trichloroacetylpyrrole –Hirshfeld...

ARTICLE *in* CRYSTAL GROWTH & DESIGN · JULY 2013

Impact Factor: 4.89 · DOI: 10.1021/cg400584w

4 AUTHORS, INCLUDING:

Agnieszka J. Rybarczyk-Pirek
University of Lodz
47 PUBLICATIONS **330** CITATIONS
SEE PROFILE

Magdalena Malecka
University of Lodz
78 PUBLICATIONS **453** CITATIONS
SEE PROFILE

Sławomir Wojtulewski
University of Bialystok
20 PUBLICATIONS **260** CITATIONS
SEE PROFILE

CRYSTAL GROWTH & DESIGN

Article

pubs.acs.org/crystal

Intermolecular Interactions of Trichloromethyl Group in the Crystal State, the Case of 2-Trichloromethyl-3*H*-4-quinazoline Polymorphs and 1-Methyl-2-trichloroacetylpyrrole–Hirshfeld Surface Analysis of Chlorine Halogen Bonding

Agnieszka J. Rybarczyk-Pirek,*[,†] Lilianna Chęcińska,[†] Magdalena Małecka,[†] and Sławomir Wojtulewski[‡]

[†]Structural Chemistry and Crystallography Group, Department of Theoretical and Structural Chemistry, University of Łódź, ul. Pomorska 163/165, 90-236 Łódź, Poland

[‡]Department of Theoretical Chemistry, University of Białystok, ul. Hurtowa 1, 15-339 Białystok, Poland

Supporting Information

ABSTRACT: Intermolecular interactions in the crystal state, a possible source of the observed polymorphism, are investigated with the use of the combined crystallographic methods, theoretical computations, and a modern approach of Hirshfeld surface analysis. Special attention is paid to a trichloromethyl group, a potential donor of halogen bonding. It is demonstrated that due to packing effects and stacking interactions, its conformation does not have to correspond to the lowest energy structure of an isolated molecule, leading to formation of different polymorphs. The analysis of Hirshfeld surfaces, in contrast to standard geometrical criterion of sum of van der Waals radii, indicates the dominant role of various chlorine intermolecular contacts into the overall molecular packing and reveals the characteristic features of the obtained fingerprint plots. These interactions, a subject of our special interest, are discussed in details in order to provide their comprehensive description by means of Hirshfeld surface analysis tools.

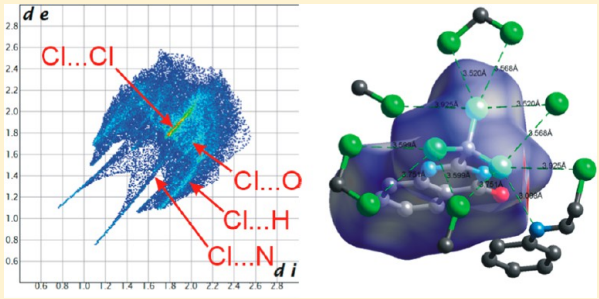

INTRODUCTION

Early studies based on crystallographic results have demonstrated that halogen atoms tend to interact with other atoms of an excess of electron charge density, playing the role of Lewis acids.[1] The resulting interactions can be strong enough to influence the aggregation of organic molecules, hence, the term halogen bonding[2] was introduced to establish its analogy with hydrogen bonding. The halogen bonding, is described by R–X···Y–Z formula,[3] where X denotes a halogen atom with an electrophilic (electron poor) region and Y another atom playing the role of a Lewis base. In the above scheme, in analogy with the hydrogen bond, the R–X group is called as a halogen-bonding donor, and Y–Z, being a nucleophilic (electron-rich) region of a molecule, is called a halogen-bonding acceptor. In recent years, halogen bonds have received much interest due to their similarity to hydrogen bonds in strength and directionality. Many researches are devoted to prove their importance in stabilizing the molecular arrangement in the solid state.[4] Halogen bonds have also been shown to be responsible for physical, chemical, and biological properties of a large number of chemical species,[2c,5] since they can bind molecules into stable large complexes and can easily be broken in experimental conditions. They are also expected to play an important role in crystal engineering, supramolecular chemistry, drug design, and new material engineering.[4c,5−7]

From the chemical point of view, the existence of halogen bonding first seemed to be a surprising phenomenon. An electronegative halogen atom should accumulate the negative charge leading to the repulsive instead of attractive interaction with the Y atom. Now, the mechanism of formation of halogen bonding is rather recognized. There are two main factors responsible for stabilization of halogen bonding: anisotropy of halogen atom electron charge density[6d,7] and HOMO/LUMO charge transfer between the interacting atoms.[1a,8] Recently, the nature of interactions between the halogen atom and several different molecules has been explained by "Bent's rule" acting between Lewis bases and acids.[9]

In accordance with theoretical investigations, the electron charge density anisotropy of a halogen atom bonded to Csp^3 carbon atom is enhanced by close proximity of other halogen atoms, especially fluorine atoms, due to sigma electron withdrawing effects.[10] This leads to a partial positive charge in the region of halogen valence sphere opposite to the covalent bond. A local deficit of an electron charge placed opposite the R–X σ bond is defined as a sigma hole (σ hole). In general, the more strongly electronegative substituents (usually other halogen atoms) bonded to the Csp^3(–X) carbon atom, the higher the electron density anisotropy observed. In turn, a methyl group

Received: April 18, 2013
Revised: July 18, 2013
Published: July 22, 2013

substituted with three halogens has been proven to be a good halogen bonding donor.[8−10]

Against this background, a trichloromethyl group has attracted our attention because of potential sigma effects on chlorine halogen bonding. In comparison with other halogens, fluorine and chlorine atoms are present in a large number of active compounds of chemical and biological importance. However, fluorine atoms in fluorocarbons are usually described as merely able to form halogen bonding because of their smaller polarizability in comparison with other halogens and a lack of a positively charged σ hole.[4c,d] On the other side, trichloromethyl-substituted compounds are in general more convenient objects of crystallographic studies than often disordered trifluoromethyl derivatives. Hence, as an object of our studies, we have chosen trichloromethyl derivatives.

As a starting point for our discussion on trichloromethyl halogen bonding and relative interactions, we present X-ray studies of two different trichloromethyl-substituted compounds: 2-trichloromethyl-3*H*-4-quinazoline **1** and 1-methyl-2-trichloroacetylpyrrole **2** (Scheme 1). We have chosen compounds that include the same potential halogen-bonding donors (a trichloromethyl group) and acceptors (a carbonyl group) in their molecules. On the other side, these two compounds differ from each other by the possibilities of hydrogen-bonding formation. In contrast to the presence of an N−H proton-donating group in molecule **1**, there are no conventional hydrogen-bonding donors in molecule **2**. As there are carbonyl groups, the same potential halogen-/hydrogen-bonding acceptors, in both molecules, we have expected that our studies also enable analysis of competition and/or cooperation processes upon halogen and hydrogen bond formation.

Scheme 1. Structural Diagrams: (a) 2-Trichloromethyl-3*H*-4-quinazoline (1) and (b) 1-Methyl-2-trichloroacetylpyrrole (2)

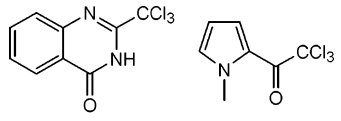

(a) (b)

The main aim of the presented work is geometrical analysis of intermolecular interactions in crystal structure, in particular involving chlorine atoms of trichloromethyl groups. It is completed by Hirshfeld surface analysis. This relatively new method allowed for the identification of individual types of intermolecular contacts and their impact on the complete packing and visualization of the shape of the molecule as it is seen by the interacting neighbors. There are only a few examples in the literature describing halogen intermolecular contacts with the use of this method[11] but no systematic analysis of Hirshfeld fingerprint plots of these interactions has been performed. There has been observed the growing interest in applications of Hirshfeld surface analysis because this approach is a very convenient tool for the exploration of different kinds of intermolecular interactions from conventional hydrogen bonds to weak π interactions and H···H contacts.[12] On the other hand, since halogen bonds are present in a large number of organic, inorganic, and organometallic crystal structures, and they are revealed to influence molecular structure of biologically active macromolecules, detailed Hirshfeld surface studies on these interactions seem to be necessary for their entire description and comparison in a variety of molecular systems. Hence, we are presenting in this paper the first detailed analysis of chlorine halogen bonds in the crystal structure with the use of a Hirshfeld

Table 1. Crystallographic Data and Structure Refinement Details

	1-orth	1-tric	2
formula	$C_9H_5Cl_3N_2O$	$C_9H_5Cl_3N_2O$	$C_7H_6Cl_3NO$
crystal system	orthorhombic	triclinic	orthorhombic
space group	*Pbca*	$P\bar{1}$	$P2_12_12_1$
unit cell (Å, deg)	a = 5.942(1)	a = 9.961(2)	a = 6.382(1)
	b = 17.846(4)	b = 10.440(2)	b = 11.442(2)
	c = 19.075(4)	c = 11.012(2)	c = 12.786(2)
		α = 97.45(3)	
		β = 103.80(3)	
		γ = 110.22(3)	
V (Å^3)	2022.8(7)	1015.0(4)	933.7(3)
Z, d_x (g/cm^3)	8, 1.730	4, 1.724	4, 1.611
μ (mm^{-1})	0.875	0.534	0.567
crystal description	light yellow plate	light yellow plate	colorless prism
crystal size (mm)	0.10 × 0.30 × 0.30	0.15 × 0.25 × 0.30	0.10 × 0.10 × 0.30
temperature	100(2) K	100(2) K	100(2) K
radiation type/λ (Å)	Mo Kα/0.71073	synchrotron/0.6	synchrotron/0.6
data collected (R_{int})	5727 (0.036)	5207 (0.022)	5458 (0.025)
θ range (deg)	3.12 to 25.02	1.65 to 22.61	2.02 to 22.60
$(\sin\theta/\lambda)_{max}$ (Å^{-1})/d (Å)	0.60/0.83	0.64/0.78	0.64/0.78
completeness (%)	99.8	97.8	99.9
data unique/$I > 2\sigma(I)$	1780/1566	4372/4330	2059/2059
parameters/restraints	140/0	280/0	110/0
goodness-of-fit on F^2	1.066	1.085	1.102
R/$wR2$ indices [$I > 2\sigma(I)$]	0.0294/0.0343	0.0228/0.0229	0.0186/0.0186
R/$wR2$ indices (all data)	0.0737/0.0764	0.0615/0.0616	0.0483/0.0483
$\Delta\rho_{max}/\Delta\rho_{min}$ (eÅ^{-3})	0.328/−0.259	0.447/−0.405	0.214/−0.264

dx.doi.org/10.1021/cg400584w | *Cryst. Growth Des.* 2013, 13, 3913−3924

Table 2. Selected Geometric Parameters for 1 Crystal Structures and Theoretical Lowest Energy Molecular Conformer (Å, deg)

	1-orth	1-tricA	1-tricB	1 (opt)
Cl3−C21	1.771(2)	1.804(1)	1.769(1)	1.814
Cl2−C21	1.784(2)	1.799(1)	1.831(1)	1.814
Cl1−C21	1.763(2)	1.767(1)	1.766(1)	1.770
C2−C21	1.531(3)	1.539(2)	1.548(2)	1.533
O4−C4	1.232(2)	1.241(2)	1.243(2)	1.216
C2−N1	1.280(3)	1.280(2)	1.285(2)	1.280
C2−N3	1.380(3)	1.383(2)	1.386(2)	1.372
C4−N3	1.385(3)	1.385(2)	1.396(2)	1.404
C2−C21−Cl1	111.2(1)	111.16(7)	112.20(9)	112.1
C2−C21−Cl2	107.7(1)	108.40(9)	108.77(8)	108.6
C2−C21−Cl3	110.9(1)	109.03(8)	108.69(8)	108.6
C2−C21−Cl2	107.7(1)	108.40(9)	108.77(8)	108.6
Cl1−C21−Cl3	108.9(1)	106.58(7)	108.29(7)	108.4
Cl1−C21−Cl2	108.6(1)	111.16(7)	109.01(7)	109.5
Cl3−C21−Cl2	109.5(1)	109.47(7)	109.87(7)	109.5
N1−C2−N3	125.5(2)	125.9(1)	126.0(1)	124.4
N1−C2−C21	118.0(2)	118.9(1)	114.8(1)	120.0
N3−C2−C21	116.3(2)	115.2(1)	119.2(1)	115.60
O4−C4−N3	121.0(2)	121.4(1)	121.7(1)	120.59
C2−N3−C4	121.7(2)	122.6(1)	122.1(1)	123.74
C2−N1−C9	117.1(2)	115.9(1)	116.3(1)	117.56
N1−C2−C21−Cl1	19.7(2)	−0.1(2)	−175.7(2)	0.0
N1−C2−C21−Cl2	−99.2(2)	−123.2(2)	−55.0(2)	−121.1
N1−C2−C21−Cl3	141.0(2)	117.7(2)	64.6(2)	121.1

surface and its corresponding fingerprint plots. In addition, a part of our study is focused on theoretical DFT calculations to obtain an additional source of information about interactions in the crystal state when compared with a gas phase.

EXPERIMENTAL SECTION

X-ray Structure Determination. Crystals suitable for X-ray measurement were obtained from commercially available reagents (Aldrich Chemical Company), which were used without further purification.

Two polymorphs of 2-trichloromethylquinazoline **1** were obtained from crystallization in different solutions: triclinic form **1-tric** (toluene) and orthorhombic **1-orth** (methanol). Crystals of 1-methyl-2-trichloroacetylpyrrole **2** were obtained after slow evaporation of the methanol solution at room temperature.

X-ray data of **1-tric** and **2** were measured with the use of synchrotron radiation at beamline F1 of the storage ring DORIS III at the HASYLAB/DESY, Hamburg, Germany. The experiments were carried out on a five-circle kappa-geometry Huber diffractometer equipped with a MAR165 CCD detector at the temperature of 100 K. Data reduction was performed with the program XDS.[13] X-ray data of **1-orth** were collected at low temperature on the Oxford Diffraction SuperNova Dual diffractometer with monochromated Mo Kα X-ray source. Data reduction and analytical absorption correction were performed with CrysAlis PRO.[14] All the three data sets were sorted and merged using XPREP.[15] The crystal structures were solved by direct methods and refined on F^2 by full-matrix least-squares procedures using SHELXL-97.[16] Positions of NH hydrogen atoms were found on the Fourier difference map and refined. Hydrogen atoms of aromatic rings and methyl groups were introduced in calculated positions with idealized geometry and constrained using a rigid body model with isotropic displacement parameters equal to 1.2 or 1.5 of the equivalent displacement parameters of the parent atoms. The molecular geometry was calculated by PARST[17] and Platon,[18] the programs implemented in WinGX system.[19] A summary of relevant crystallographic data is given in Table 1.

Theoretical Computations. Quantum chemical calculations were performed to study the structure and relative stability of different conformers of the title compounds. All the theoretical calculations were performed with the Gaussian 09 sets of codes,[20] utilizing density functional theory methods (DFT). Two kind of calculations were performed. First, the molecular geometries taken from X-ray studies, with normalized hydrogen bond lengths, were entered into single-point calculations with the use of the hybrid functional of Becke with Lee, Yang, and Parr gradient correction (B3LYP) and 6-311++G(d,p) atomic basis sets. Then, using the same level of approximation, the molecular geometries were fully optimized starting again with the crystal structure molecular geometry. In addition, the conformational analysis was performed with series of molecular geometry optimization, including a 10° step scan of the Cl−C−C−N/O torsion angle to identify energy stable conformers arising during trichloromethyl group rotation.

Hirshfeld Surface Analysis. The Hirshfeld molecular surfaces were generated using CrystalExplorer 3.0[21] based on results of X-ray studies. During the calculations, bond lengths to hydrogen atoms were normalized to standard neutron values (C−*H* = 1.083 Å, O−*H* = 0.983 Å, N−*H* = 1.009 Å)[22] in order to ensure the internal consistency and independence of results from the crystal structure refinement method. For comparison of intermolecular interactions scheme in crystal structures, the normalized contact distances, d_{norm},[21a] based on van der Waals radii, were mapped into the Hirshfeld surfaces. In the color scale, negative values of d_{norm} are visualized by the red color, indicating contacts shorter than the sum of van der Waals radii. The white color denotes intermolecular distances close to van der Waals contacts with d_{norm} equal to zero. In turn, contacts longer than the sum of van der Waals radii with positive d_{norm} values are colored with blue. The Hirshfeld surface fingerprint plots were generated using d_i (distance from the surface to the nearest atom in the molecule itself) and d_e (distance from the surface to the nearest atom in the another molecule) as a pair of coordinates, in intervals of 0.01 Å, for each individual surface spot resulting in two-dimensional histograms. A color gradient in the plots ranging from blue to red represents the proportional contribution of contact pairs in the global surface.

RESULTS AND DISCUSSION

The Crystal Structure of 2-Trichloromethyl-3*H*-4-quinazoline. The crystals of 2-trichloromethyl-3*H*-4-quinazo-

dx.doi.org/10.1021/cg400584w | Cryst. Growth Des. 2013, 13, 3913−3924

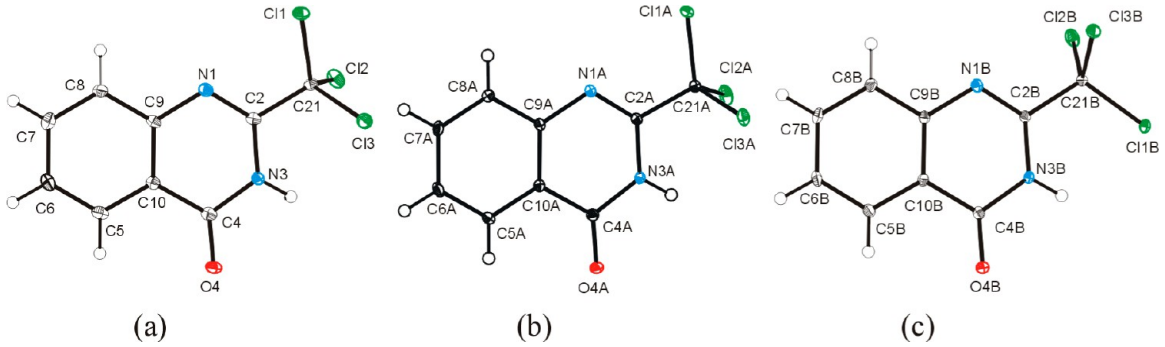

Figure 1. Molecular drawings indicating conformational differences of 2-trichloromethyl-3*H*-4-quinazoline: (a) **1-orth**, (b) **1-tricA**, and (c) **1-tricB**. Atomic displacement ellipsoids are drawn at the 40% probability level.

line obtained from two different solutions: toluene and methanol, represent two polymorphs: orthorhombic **1-orth** and triclinic **1-tric**, respectively (Table 1). There are two symmetrically independent molecules assigned as **A** and **B** in the crystal structure of **1-tric**. When comparing bond lengths and angles in molecules of **1-orth**, **1-tricA**, and **1-tricB**, there are no meaningful differences (Table 2). However, in the three-dimensional structures there are significant differences in conformation of the trichloromethyl group with respect to the heterocyclic aromatic ring (Figure 1).

The arrangement trichloromethyl substituent atoms and, in general, the molecular conformation can be best defined by the N1−C2−C21-Cl1 torsion angle, where absolute values vary from 0.1(1)° **1-tricA** through 19.7(2)° **1-orth** to 175.7(1)° **1-tricB**. Another observation of the trichloromethyl substituent is differentiation of three C−Cl covalent bonds lengths. In the case of all three molecules, evidently, the shortest are C21−Cl1 bonds with chlorine atoms in close positions to the condensed ring planes. Such a situation was previously observed in the case of the trichloroacetic anion crystal structure.[23] Distances between positions of Cl1 atoms and the quinazoline least-squares planes are changing from 0.258(1)Å in **1-tricB** to 0.397(1)Å in **1-orth**, while for other chlorine atoms, these distances are all above 1 Å.

In the all crystal structures of 2-trichloromethyl-3*H*-4-quinazoline, the molecules are linked into similar dimers by a pair of N3−H3···O4 intermolecular hydrogen bonds, resulting in the $R_2^2(8)$ motif, according to the graph-set notation[24] which is presented in Figure 2.

For **1-orth** dimers are formed by two molecules related by the crystallographic inversion, while in the case of **1-tric** they are built of a pair of independent **A** and **B** molecules showing inversion pseudosymmetry in position x = 0.20, y = 0.71, z = −0.03, which can be characterized by RMS fit parameters[18] equal to 0.006 Å for bond fit and 1.4° for angle fit, respectively (Figure S1 of the Supporting Information).

The analysis of intermolecular distances indicated the existence of some Cl···Cl, Cl···N, and Cl···π contacts shorter than the sum of van der Waals radii[25] in both crystal structures, which are listed in Table 3.

It is now well-established that close contacts between halogens and nucleophiles, leading to halogen-bonding formation, are distributed approximately along the covalent C−X bond with C−X···Y angles in the range of 150−180°. Hence, halogen bonding is regarded as a very directional interaction.[3,4] On the other hand, when halogens are interacting with electrophiles, like in the case of D−H···X hydrogen bonding, the respective angles should be in the range of 90−120°. Detailed inspection of the chlorine intermolecular contacts, with the use of the angular

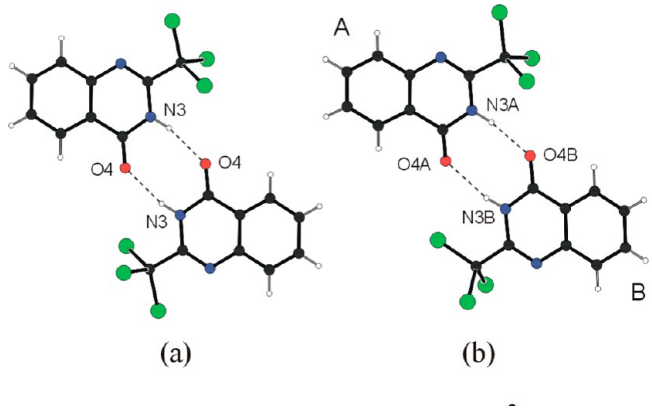

Figure 2. N−H···O hydrogen bonding $R_2^2(8)$ motif in 2-trichloromethyl-3*H*-4-quinazoline crystal structures: (a) **1-orth**, molecules related by an inversion and (b) **1-tric**, two symmetrically independent molecules.

criterion, indicates that only some of them may be regarded as halogen bonds, while the rest are interactions of other types. As a typical halogen bond, they should then be classified as a C21−Cl3···N1 interaction in **1-orth** and C21B−Cl1B···Cl3A, C12B−Cl2B···π (with C5A−C6A−C7A−C8A−C9A−C10A phenyl ring) and C21A−Cl3A···π (with the C5B−C6B−C7B−C8B−C9B−C10B phenyl ring) interactions in **1-tric**, respectively. C−Cl···Cl halogen bonds are common in crystal structures and widely analyzed in literature.[27] In contrast, C−Cl···π (or in general C−X···π) halogen bonds are not so often observed in crystal structures, but they are not unique ones.[28] For more detailed analysis of the observed geometrical parameters of halogen bonds, we have performed a search of the Cambridge Structural Database.[29] The analyzed parameters are in the range of typical values observed for similar crystal structures, except for a very short Cl···N distance, which in turn cannot be reliably compared as there are only three similar crystal structures found (Table S1 of the Supporting Information).

Further comparative analysis of the 2-trichloromethyl-3*H*-4-quinazoline polymorphic structures let us conclude that the structure of orthorhombic polymorph **1-orth** is built of two kind of layers alternating along crystallographic *b* direction: a layer of closely packed aromatic condensed rings connected by hydrogen N−H···O bonds and a layer of chlorine atoms of trichloromethyl groups (Figure 3). Similar layers can be indicated in the structure of the triclinic **1-tric** form. In addition, there are stacking interactions between the heterocyclic ring of molecule **B** and the phenyl ring of molecule **A**, with interplanar and centroid−

dx.doi.org/10.1021/cg400584w | *Cryst. Growth Des.* 2013, 13, 3913−3924

Table 3. Geometry of Intermolecular Hydrogen (D−H A) and Halogen (D−X Y) Bonds for 1 and 2 Crystal Structures

D−H/X A/Y	d(D−H/X) (Å)	d(H/X...A/Z) (Å)	d(D...A/Y) (Å)	<D−H/X···A/Y (deg)	symmetry
		1-orth			
N3−H3···O4	0.86(3)	2.02(3)	2.856(2)	167(2)	$2-x, 2-y, 1-z$
C21−Cl3···N1	1.771(2)	3.098(2)	4.677	146.45(8)	$1+x, y, z$
		1-tric			
N3A-H3A···O4B	0.87(2)	1.94(2)	2.793(2)	170(2)	$x, y, 1+z$
N3B−H3B···O4A	0.85(2)	2.08(2)	2.905(2)	165(2)	$x, y, -1+z$
C21B−C1B···Cl3A	1.766(1)	3.4935(8)	5.106(2)	150.64(5)	$-x, 1-y, 1-z$
C21A-Cl3A···πB[a]	1.804(1)	3.545(1)	5.251(2)	156.76(5)	$-x, 2-y, 1-z$
C21B−Cl2B···πA[a]	1.831(1)	3.644(1)	5.352(2)	154.16(5)	$1-x, 1-y, 1-z$
		2			
C6−Cl2···O1	1.784(1)	2.941(1)	4.715(1)	172.39(5)	$1+x, y, z$
	1.778(3)[b]	3.047(2)[b]	4.801(3)[b]	168.6(1)[b]	$1+x, y, z$

[a]Phenyl ring; geometric parameters calculated for ring center of gravity. [b]Previous room temperature (T = 293 K) study of **2**.[26]

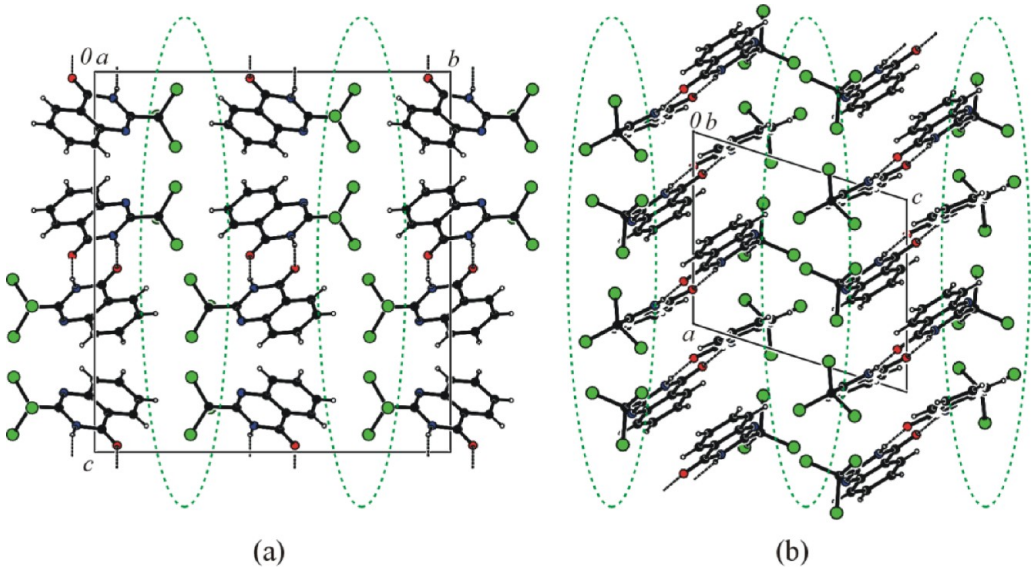

Figure 3. Crystal packing of 2-trichloromethyl-3*H*-4-quinazoline revealing layered nature of the structures: (a) **1-orth** and (b) **1-tric**. Chlorine layers are indicated by green dotted lines.

Table 4. Selected Geometric Parameters for 2 Crystal Structure and Theoretical Lowest Energy Molecular Conformer (Å, deg)

	2 (T = 100 K, this study)	**2** (T = 293 K)[25]	**2** (opt)
Cl1−C6	1.788(1)	1.767(2)	1.806
Cl2−C6	1.784(1)	1.778(2)	1.806
Cl3−C6	1.770(1)	1.763(2)	1.780
C5−O1	1.223(2)	1.209(3)	1.214
C5−C6	1.581(2)	1.564(3)	1.586
C1−N1	1.400(2)	1.391(3)	1.398
O1−C5−C1	124.9(1)	124.7(2)	123.9
N1−C1−C5	120.8(1)	121.2(2)	120.8
Cl3−C6−Cl2	108.25(7)	107.9(1)	108.70
Cl3−C6−Cl1	108.25(7)	107.6(1)	108.70
Cl2−C6−Cl1	110.37(7)	110.7(1)	109.86
C1−C5−C6−Cl1	−64.0(1)	−61.0(2)	−60.5
C1−C5−C6−Cl2	57.7(1)	60.2(2)	60.5
C1−C5−C6−Cl3	177.2(1)	179.1(2)	180.0

centroid distances equal to 3.408(1)Å and 4.049(1) Å, respectively. The dihedral angle between the corresponding ring planes is equal to 13.3(1)°.

As was mentioned, the two types of **1-tric** molecules, **A** and **B**, differ from each other by the trichloromethyl group conformation. If only one conformer was involved in building the crystal structure, it would produce, due to stacking interactions, many contacts much shorter than the sum of the van der Waals radii consequently leading to strong steric repulsion, as will be described in detail.

dx.doi.org/10.1021/cg400584w | *Cryst. Growth Des.* 2013, 13, 3913−3924

Crystal structure of 1-methyl-2-trichloroacetylpyrrole. The crystal structure of 1-methyl-2-trichloroacetylpyrrole **2** was previously determined at room temperature.[26] A very interesting feature of **2** is an existence of very short C6−Cl2···O1 halogen-bonding intermolecular contacts. It is frequently indicated that upon formation of the R−X···Y−Z halogen bond, in analogy to the formation of a hydrogen bond, an elongation of a R−X donor covalent bond may be expected.[3] In fact, such a situation was observed in **2** in our previous study, hence, the low temperature crystal structure redetermination has been performed to clarify this observation (Figure S2 of the Supporting Information). Moreover, to make accurate and meaningful comparisons of related crystal structures, it is essential to use structural data that were collected under similar conditions. For this purpose, in this paper we compare crystal structures of **1** and **2** determined in the same temperature.

The present study provides more precise information about atom positions (Table 4); however, it does not confirm the room temperature results of C6−Cl2 bond elongation upon formation of the halogen bond. In the comparison with the previous studies, the Cl2···O1 distance is slightly shorter, even in comparison with the CSD (Table S1 of the Supporting Information), with elongation of the O1−C5 bond in the carbonyl group. There is also similar differentiation of C−Cl bond lengths in the trichloromethyl substituent, as observed for polymorphs of **1**.

In general, this study has confirmed that for 1-methyl-2-trichloroacetylpyrrole crystal structure, the most important intermolecular interaction is the C6−Cl2···O1 halogen bonding, as presented in Figure 4.

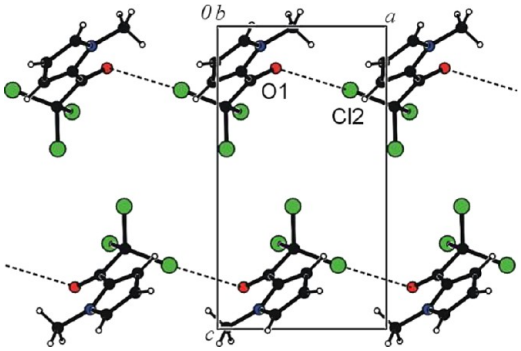

Figure 4. C−Cl···O halogen-bonding chain motif in the 1-methyl-2-trichloroacetylpyrrole crystal structure. Other molecules within the unit cell are omitted for clarity.

Conformational Analysis. In the crystal structures of **1**, polymorphs of three various molecular conformers, namely **1-orth**, **1-tricA**, and **1-tricB**, are found. The differences in their conformations are described by the N1−C2−C21−Cl1 torsion angles. The existence of three different molecular conformations in the crystal state, as well as the observed polymorphism, turn our attention to crystal packing effects, intermolecular contacts, and their role in the relative stability of each molecular structure. To have a more detailed insight into this problem, we have computationally studied the trichloromethyl group rotation process. A series of molecular geometry optimization have been performed with the use of the DFT method. By changing the Cl−C−C−N/O torsion angle in the step of 10° (for the molecules of both compounds **1** and **2**), we scanned changes of molecular energy (Figure S3 of the Supporting Information). During the rotation of the trichloromethyl group, three energy stable conformers, of the similar energies, occur for both compounds. The calculated energy barrier for the rotation along the C−C bond is found to be around 1.6 kcal/mol for **1** and 4.7 kcal/mol for **2**. The lower energy barrier of **1** may suggest why there are three different conformers in the crystal state. Interestingly, in the cases of molecules **1-tricA** and **2**, the observed molecular conformations correspond to the lowest energy conformers found for free molecules. For **1-orth**, the rise of energy caused by slight rotation of trichloromethyl substituent is compensated probably by crystal field effects due to the formation of a layered structure and weak halogen bonds. Surprisingly, the structure of the **1-tricB** molecule resembles a conformation very close to the rotation transition state. To explain this problem, we have compared results of the single point and optimized geometry calculations. The representative geometric parameters of the lowest energy conformers **1** (opt) and **2** (opt) are compared with experimental results in the Tables 2 and 4, respectively.

The energy difference between **A** and **B** conformers as obtained from single point calculations is equal to 1.99 kcal/mol. Further comparison of the obtained energies is presented in Table 5.

Table 5. Total and Relative Energies of Molecular Conformers from Single Point Calculations (sp) and Optimized Geometry Calculations (opt)[a]

	E (a.u.)	ΔE (kcal/mol)
1-orth (sp)	−1911.5177	−2.04
1-tricA (sp)	−1911.5174	−2.22
1-tricB (sp)	−1911.5142	−4.21
1 (opt)	−1911.5209	0
2 (sp)	−1781.0813	−1.39
2 (opt)	−1781.0835	0

[a]Relative energies are calculated as energy differences in relation to the optimized structure: $\Delta E = E_{opt} - E$.

The most important is the fact that during geometry optimization, the high energy **1-tricB** is unstable on a free molecule and collapses into the low-energy conformer, corresponding to **1-tricA** conformation. On the basis of these results, it seems that described earlier **1-tric** stacking interactions may be an important factor stabilizing unusual molecular conformation.

To answer why the unstable, higher energy conformer is observed in the crystal state, we have made a simulation of the **1-tric** crystal structure as it were built from only low energy molecular conformers. We have imposed the conformation of trichloromethyl substituent in the **B** molecule as calculated for the lowest energy conformer (corresponding to the **A** molecule). The simulated positions of chlorine atoms are given in Table S3 of the Supporting Information, and obtained in that way, crystal packing is presented in Figure 5. This simulation allowed us to calculate the interatomic distances between nearest neighboring atoms to discern possible sources of strong steric interaction responsible for a change of molecular configuration upon crystallization.

Our analysis has indicated several very short interatomic distances between simulated positions of the chlorine and other atoms of aromatic fragments of neighboring molecules. When those distances compared with the sum of the van der Waals radii, it became clear that the existence of a such conformation in the crystal state should lead to strong repulsion between molecules.

dx.doi.org/10.1021/cg400584w | *Cryst. Growth Des.* 2013, 13, 3913−3924

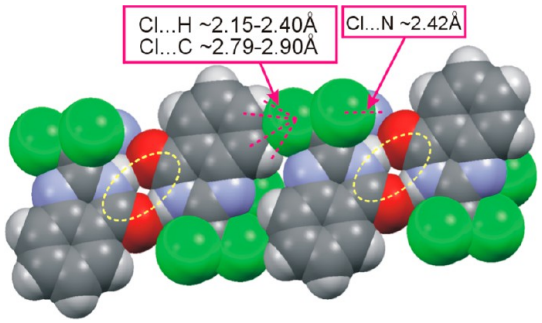

Figure 5. Simulation of the **1-tric** tetramer in the crystal structure with the theoretically calculated low energy conformer placed in the position of molecule **B**. Very close interatomic contacts with chlorine atoms (much shorter than the sum of van der Waals radii) which cause steric hindrance are indicated with red dotted lines. $R_2^2(8)$ hydrogen-bonding motifs are indicated with yellow dotted lines.

Altogether, we have found 13 interatomic distances involving three chlorine atoms that are much shorter than the sum of van der Waals radii (Table S4 of the Supporting Information). This is the reason for the crystallization process to favor the conformer with the higher energy corresponding to the structure of molecule **B**. Hence, it led to the conclusion that upon formation of a stable crystal structure, short intermolecular contacts are avoided by internal conformational rearrangement, leading to a molecular conformer **B** that seemed previously to be unfavorable because of its higher energy in the gas phase.

σ-Holes on Molecular Electrostatic Potential Surfaces. To get an overview of the complete intermolecular interaction and their role in the packing scheme, we have decided to analyze molecular surfaces of the investigated compounds. Among many others, the Hirshfeld surfaces have been proven to identify intermolecular interactions in the crystals very reliably.[21,30] On the other side, another valuable tool commonly used in the analysis of intermolecular interactions is the electrostatic potential which can be mapped on the molecular surface. It is especially interesting in the case of chlorine atoms, as one can expect an occurrence of the chlorine σ holes.

The visualizations of the electrostatic potential (Figure 6) were obtained as a result of the theoretical single point DFT calculations based on crystal state geometries with normalized lengths to hydrogen atoms. For a suitable comparison of all investigated molecules and molecular conformers, we have taken the same isovalue of electron density for creation of molecular surfaces and the same internal colored scale of electrostatic potential as presented in the figures.

For all the molecules, there are shown negative electrostatic potential isosurface areas accumulated around oxygen atoms of carbonyl groups and, partly, in a surrounding of nonsubstituted heterocyclic nitrogen atoms in **1**. In turn, green color around the electronegative chlorine atoms indicates neutral charge on the molecular surface, excluding clearly visible areas of local deficit of an electron charge placed opposite the C−Cl bonds which correspond to σ holes.

For the molecules which correspond to the lowest energy gas-phase conformations (**1-tricA** and **2**), the calculated electrostatic potentials show the highest electron-deficient regions of chlorine atoms. It can be connected with the fact that only in these two crystal structures do we find typical halogen C−Cl···O/N bonds of very short intermolecular distances. These observations support the directional nature of the observed halogen bonds, indicating that the localization of the highest positive electrostatic potential regions of halogens (σ holes) by theoretical calculations may be a useful step in the prediction of halogen bonding in crystal structures.

Intermolecular Interactions Analysis with the Use of Hirshfeld Surfaces. The molecular Hirshfeld surface represents the area where molecules come into contact, therefore, its analysis gives the possibility of obtaining additional insight into the intermolecular interactions in the crystal state. Figure 7 depicts the Hirshfeld surfaces of compounds **1** (both polymorphic forms) and **2**. For the visualization, we have used a mapping of the normalized contact distance, d_{norm}. Its negative value enables identification of molecular regions of great importance for intermolecular interactions.

In all surfaces of 2-trichloromethyl-3*H*-4-quinazoline (**1**), regions of N−H···O hydrogen bonds visualized by large red circle areas are seen near the oxygen and NH hydrogen atoms. Some red spots near chlorine atoms connected with the halogen bonds are also clearly seen: C21−Cl3···N1 in **1-orth**, C21B−C1B···Cl3A in **1-tric**, and C6−Cl2···O1 in **2**, respectively. Interestingly, in the presented case, the analysis of the d_{norm} parameter does not give straightforward evidence of the existence of C−Cl···π halogen bonds.

A comparison of the obtained surfaces let us also notice the similarities between the most polarized areas which were shown in the mapped electrostatic potential and areas of the intermolecular contacts indicated in the Hirshfeld surfaces. It is mostly seen for strong N−H···O hydrogen bonds and C−Cl···O/N halogen bonds and can be treated as evidence of electrostatic character of these interactions.

Figure 8 presents Hirshfeld surface fingerprint plots. The dominant interactions between atoms of neighboring molecules are shown as the bright areas colored from green through yellow to red.

All the four figures show typical motifs recognized as two sharp distinct spikes in the bottom left area due to the presence of O···H interactions, even though there is no classic hydrogen bonding in **2**. In turn, for **1**, the corresponding motifs are typically elongated in the direction of the left bottom corner, indicating existence of short and strong N−H···O hydrogen bonds.

The planar structure of 4-quinalozoline skeleton provides both geometric and electronic conditions to enable stacking $\pi\cdots\pi$ interactions in the **1-tric** crystal structure. A characteristic hint toward significant stacking interactions is the central marker formed by C···C, C···N, C···O, and likewise contacts which represent the $\pi\cdots\pi$ interactions. However, in all the presented plots, there are sharp, orange-red stripes of the diagonal line symmetry which have main contribution from Cl···Cl contacts masking possible $\pi\cdots\pi$ stacking. Moreover, this motif is a common feature of all the molecules analyzed here, also known for other chlorocarbons.[21a,30] What is most important, it occurs independently of the molecular structure, possibilities of hydrogen and halogen bonding formation, or layered nature of a crystal structure. Hence, the observed Cl···Cl contacts appear to play an important role in the overall interactions scheme.

There are also other regions of relatively large spot intensity corresponding to other specific intermolecular chlorine contacts. Among them there are pairs of two sharp spikes associated with Cl···O contacts, which are especially long in the case of **2**, the structure mainly governed by C6−Cl2···O1 halogen bonding. In this case, the fingerprint for Cl···O contacts looks very much like hydrogen-bonding patterns. Moreover, similar elongation of characteristic hydrogen-bonding motifs connected with a shortening of H...O/N intermolecular distance was also

dx.doi.org/10.1021/cg400584w | *Cryst. Growth Des.* 2013, 13, 3913−3924

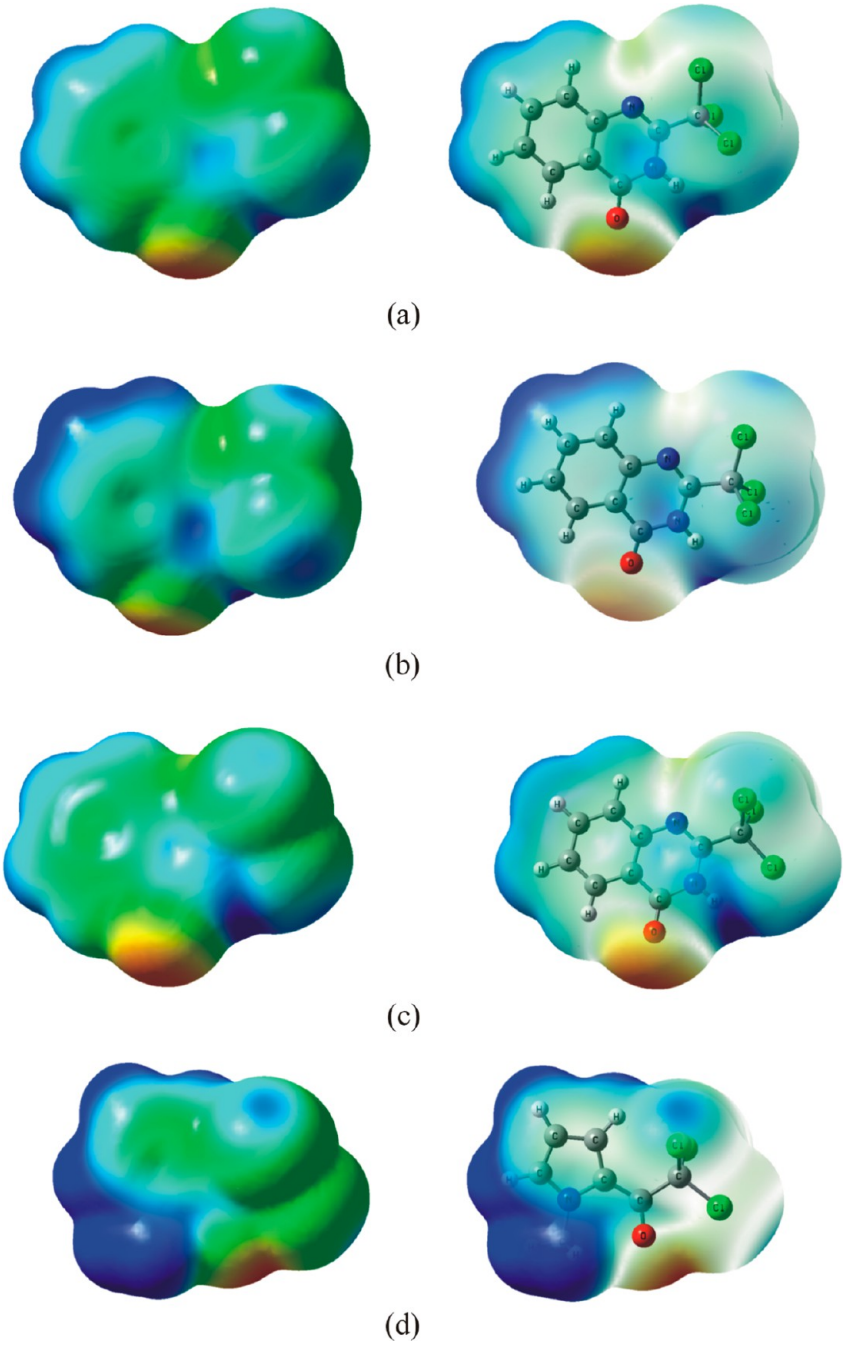

Figure 6. Electrostatic potentials mapped on the 0.002 au molecular isosurface of the electron density: (a) **1-orth**, (b) **1-tricA**, (c) **1-tricB**, and (d) **2**. Left sides of the drawings present opaque surfaces with the colored scale which correspond to values ranging from −0.05 (red) to +0.03 (blue) [Hartree], and right sides of the drawings present transparent surfaces, indicating atom positions.

observed.[21a] In turn, spikes corresponding to the Cl···N contacts are rather broad, resulting from lowering of the contact angle. Again, as in the case of C−Cl···O halogen bonds, we can observe elongation of Cl···N spikes pointing toward the bottom left of the plot upon formation of a typical halogen bond of C11−Cl3···N1 in **1-orth**.

Remarkable differences between polymorphs **1-orth** and **1-tric** can be seen by inspecting H···H regions (Figure S4 of the Supporting Information). As there are always contacts between terminal molecular atoms, the shape of 2D fingerprint plot areas and spot intensities are related to the mutual arrangement of molecules in the crystal state and, hence, they can be treated as a sign indicating differences between the polymorphic structures. The **1-tric** structure exhibits broad areas of these contacts localized in the left bottom corners, which are absent in the case of **1-orth**. We can observe that the fingerprint plots of **1-tricA** and **1-tricB** are more similar to each other than then they are to **1-orth**, despite the fact that both crystal structures are built of atomic layers stabilized by the same type of N−H···O hydrogen bonding. Thus, it confirms the statement that the shape of the fingerprint plot is closer to the crystal structure itself than to an individual molecular structure.[30b]

By decomposing the fingerprint plots to any arbitrary chosen contact type, it is possible not only to allocate the fingerprint features but also to obtain a percentage of surface coverage for the individual interaction types. Figure 9 shows the contributions

dx.doi.org/10.1021/cg400584w | *Cryst. Growth Des.* 2013, 13, 3913−3924

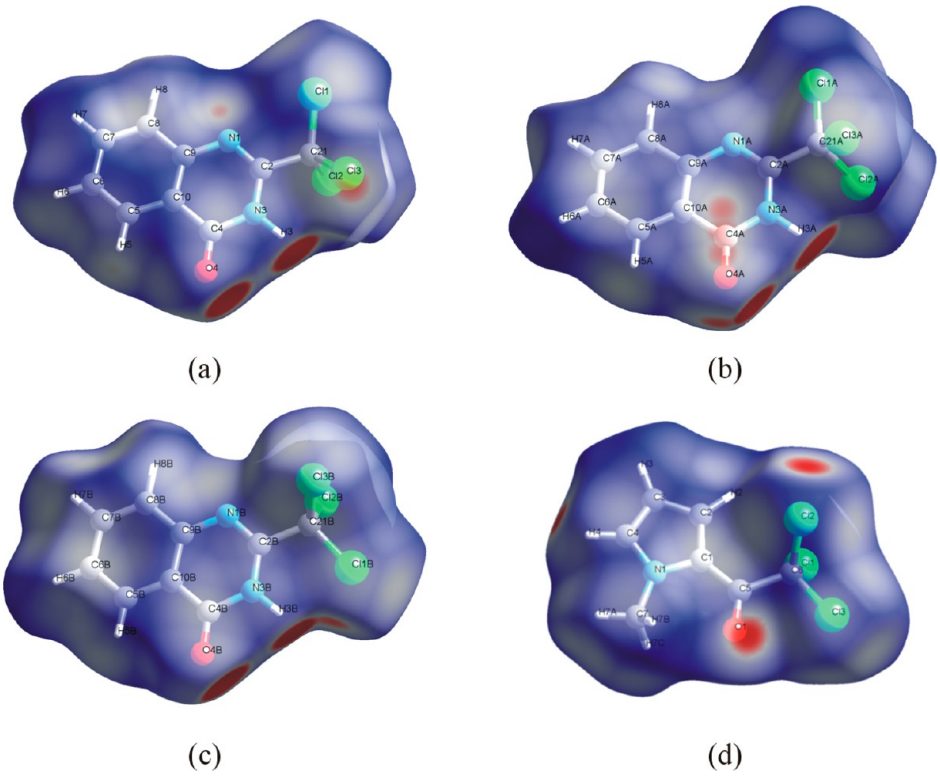

Figure 7. Molecular Hirshfeld surfaces mapped with d_{norm} with the colored scale which corresponds to values ranging from −0.25 Å (red) to 1.0 Å (blue): (a) **1-orth**, (b) **1-tricA**, (c) **1-tricB**, and (d) **2**.

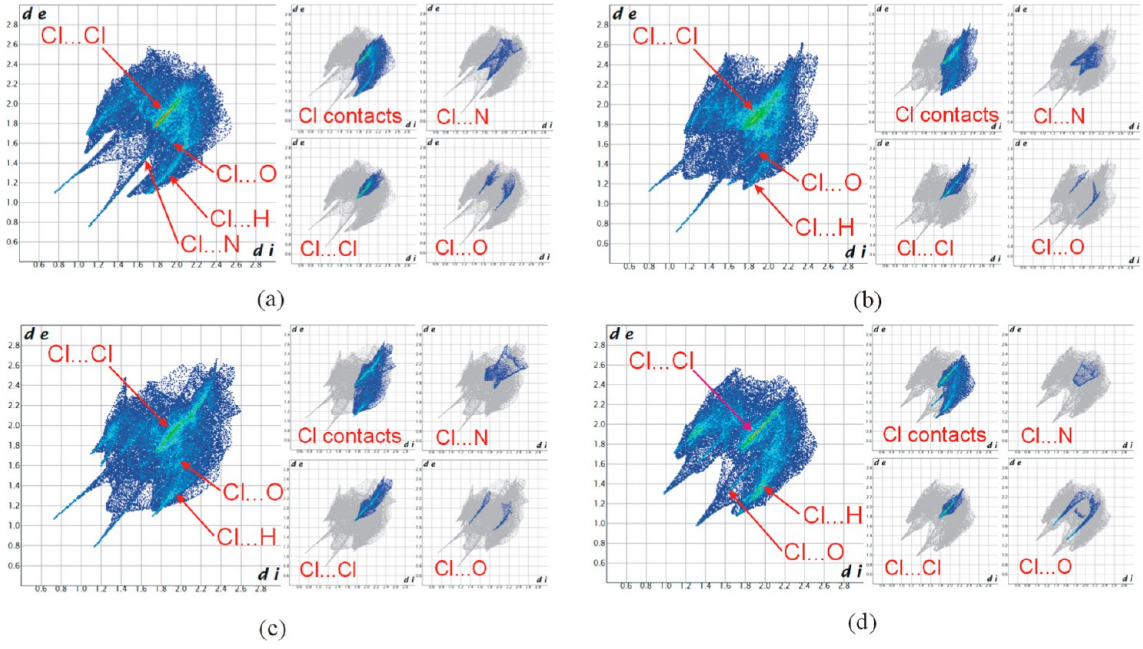

Figure 8. Hirshfeld surface 2D fingerprint plots indicating chlorine intermolecular contacts: (a) **1-orth**, (b) **1-tricA**, (c) **1-tricB**, and (d) **2**.

of various interaction types in the whole Hirshfeld surface for all the investigated molecular and crystal structures.

Surprisingly, the decomposition of the fingerprint plots indicates that chlorine intermolecular contacts cover more than half of the whole Hirshfeld surface in all the cases. It may be caused by relatively large van der Waals radii of chlorine atoms. Some of the shortest chlorine intermolecular contacts, with distances very close to the sum of the van der Waals radii (3.5 Å for Cl···Cl, 3.3 Å for Cl···N, and 3.27 Å for Cl···O), are presented in the Figure 10.

The largest contribution of chlorine contacts is observed for **2**, a compound with the relatively smallest number of atoms in the molecule. With the exclusion of terminal hydrogen atoms, among chlorine contacts, the most important are the Cl···Cl ones mentioned, even in the case of **2**, where the crystal structure seemed to be mainly governed by C−Cl···O halogen bonds.

dx.doi.org/10.1021/cg400584w | *Cryst. Growth Des.* 2013, 13, 3913−3924

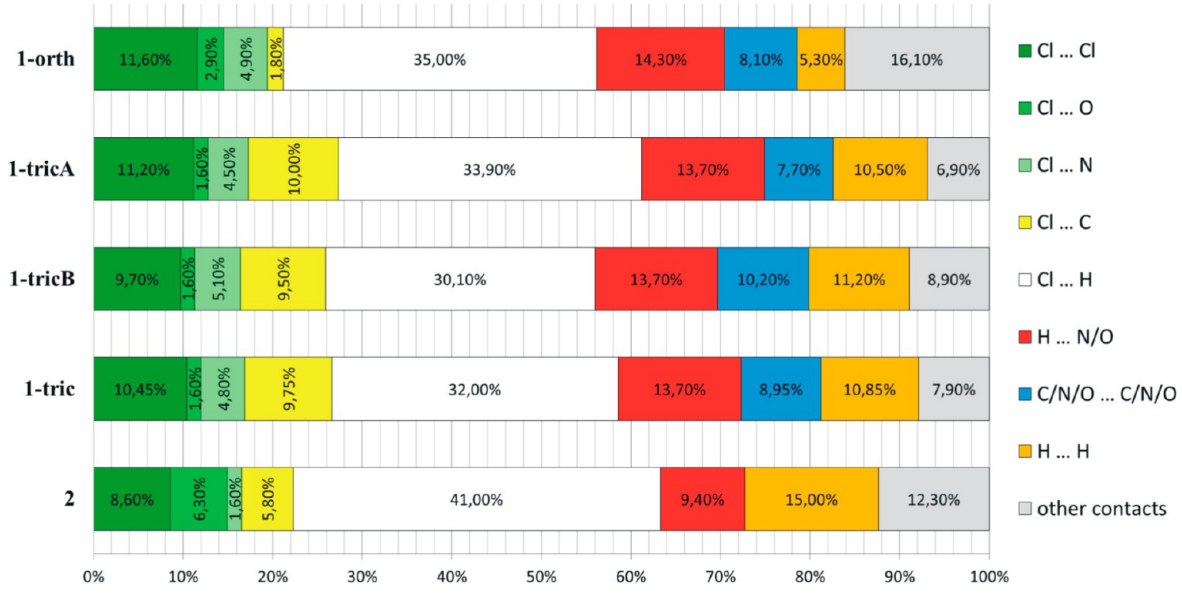

Figure 9. Distribution of intermolecular contacts on the base on Hirshfeld surface analysis.

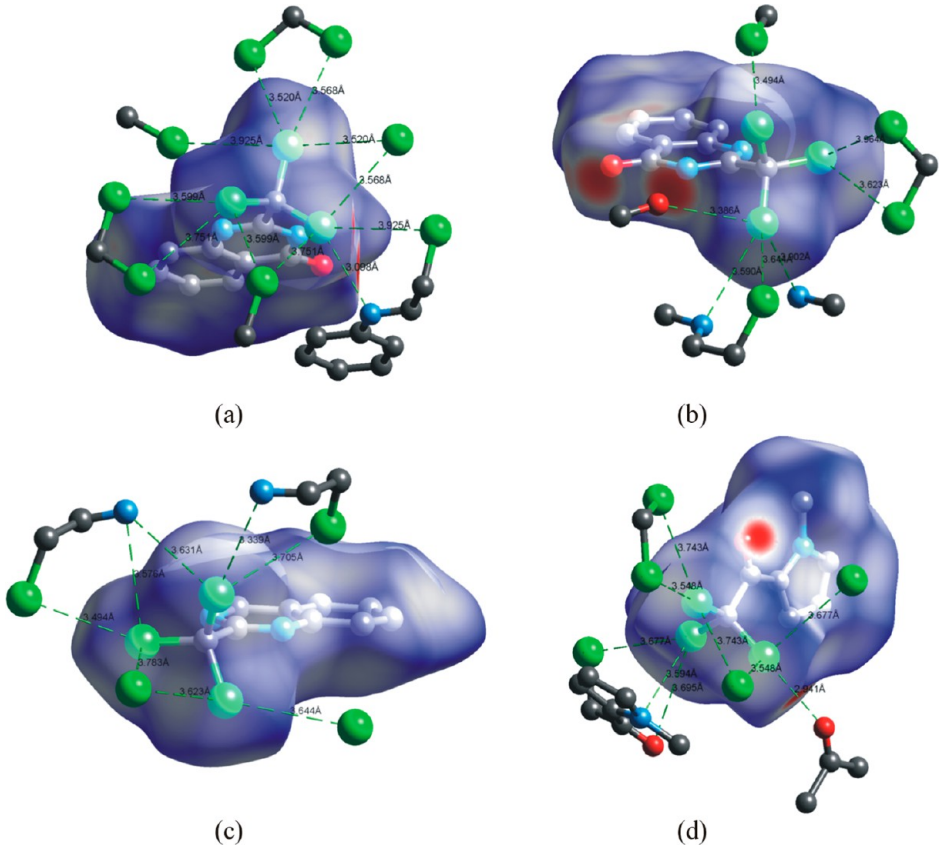

Figure 10. Short chlorine Cl···Cl, Cl···N, and Cl···O intermolecular contacts presented with d_{norm} mapped Hirshfeld surfaces: (a) **1-orth**, (b) **1-tricA**, (c) **1-tricB**, and (d) **2**.

Interestingly, for **1-tric**, quinazoline polymorph Cl···C contacts comprise about 10% of the whole surface what is evidently larger than corresponding contributions found for the other investigated structures. This feature should be attributed to the presence of C−Cl···π halogen bonds being at the same time confirmation of the existence of this kind of intermolecular interaction from the Hirshfeld surface analysis.

The proportion of N/O···H interactions of about 14% is very similar for both polymorphic structures of **1**, due to the existence of strong N−H···O hydrogen bonds, and as can be expected, evidently larger in comparison with **2**.

CONCLUSIONS

In this article, we have demonstrated that results of experimental crystallographic studies combined with the Hirshfeld surface

dx.doi.org/10.1021/cg400584w | *Cryst. Growth Des.* 2013, 13, 3913−3924

analysis approach and quantum-chemical calculations can provide an interesting insight into the crystal structure as is seen by the interacting neighboring molecules. In the analyzed quinazoline derivative crystal structures, the highly directional N−H···O═C hydrogen bonding is a preferred interaction to C−Cl···O═C halogen bonding. Nevertheless, in the absence of typical hydrogen-bonding donors, as for the pyrrol derivative, the latter one turned out to be the most important interaction stabilizing the crystal structure.

The comparative analysis of polymorphic structures confirmed that the molecular conformer observed in the crystal does not need to be the lowest energy conformer in the gas phase. In the triclinic polymorph, the trichloromethyl group conformation, representing transition state in process of molecular rotation, minimizes the repulsion between neighboring molecules and enables stacking interactions stabilizing the crystal structure.

Our studies show that not only hydrogen bonds and stacking interactions but also several chlorine intermolecular contacts, among them typical halogen bonds, can be indicated as forces driving molecular arrangement and crystal packing. Especially valuable information about chlorine interactions comes from Hirshfeld surface analysis. In all investigated crystal structures above, more than 50% of intermolecular contacts are associated with chlorine atoms and among them can be distinguished Cl···Cl, Cl···O, Cl···N, and Cl···π halogen bonds. Moreover, C−Cl···O/N halogen bonds, in contrast to the C−Cl···Cl/π interactions, can be easily recognized by analysis of the d_{norm} parameter. In turn, the information about the latter ones can be obtained by the inspection of percentage of contacts distribution over the Hirshfeld surface.

By decoding in 2D fingerprint plots, we have indicated characteristic areas associated with the specific type of chlorine contacts. All the presented plots show typical features for the Cl···O/N/Cl chlorine intermolecular contacts. The C−Cl···O halogen bonds are represented by two distinct, long, sharp parallel peaks (i.e., similar patterns as known for N/O−H···O hydrogen bonds). For Cl···N interactions, there is observed a rather broad, central area of spots divided into two peaks upon formation of the C−Cl···N halogen bonding. In contrast, for Cl···Cl, contacts are represented by one long and sharp single diagonal line of great spot intensity. Moreover, upon formation of all types of C−Cl···O/N/Cl halogen bonds, characteristic motifs of intermolecular contacts are elongated in the direction of the left bottom corner of the plot.

This study did not confirm expected connection between formation of halogen bonding and C−Cl donor bond elongation. However, lack of such an observation may be caused by existence of many various intermolecular chlorine contacts of the distances close to the sums of van der Waals radii, as indicated by Hirshfeld surface analysis, which may also affect the length of covalent C−Cl bonds.

■ ASSOCIATED CONTENT

Supporting Information

Crystallographic data for **1-orth**, **1-tric**, and **2** (CIF files; CCDC 930973−930975 reference numbers), geometrical parameters of chlorine halogen bonds derived from the Cambridge Structural Database, atomic coordinates of theoretically optimized molecules **1** and **2**, set of short Cl interatomic distances in the simulated **1-tric** crystal structure, energy as a function of the Cl−C−C−N/O angle in **1** and **2**, Hirshfeld surface 2D fingerprint plots for **1** polymorphs. This material is available free of charge via the Internet at http://pubs.acs.org.

■ AUTHOR INFORMATION

Corresponding Author

*E-mail: agnesr@uni.lodz.pl. Tel: +48 42 635 57 40. Fax: +48 42 635 57 44.

Notes

The authors declare no competing financial interest.

■ ACKNOWLEDGMENTS

The Oxford Diffraction SuperNova Dual diffractometer (S.W.) was funded by the EFRD as part of the Operational Programme Development of Eastern Poland 2007−2013, project: projects I-20090042 and EC at the light source DORIS III at/DESY, Hamburg, Germany. The research leading to these results has received funding from the European Community's Seventh Framework Programme (FP7/2007-2013) under Grant 226716. The theoretical computations were performed in Academic Computer Centre CYFRONET AGH. Authors thank Dr Carsten Paulmann for assistance in synchrotron experiments (DESY/HASYLAB). A.J. Rybarczyk-Pirek thanks Prof. Marek Z. Zgierski for his help and discussion. A.J. Rybarczyk-Pirek and L. Chęcińska are grateful to Prof. Mark Spackman for helpful discussion.

■ REFERENCES

(1) (a) Ramasubbu, N.; Parthasarathy, R.; Murray-Rust, P. *J. Am. Chem. Soc.* **1986**, *108*, 4308−4314. (b) Price, S. L.; Stone, A. J.; Lucas, J.; Rowlands, R. S.; Thornley, E. *J. Am. Chem. Soc.* **1994**, *116*, 4910−4918. (c) Lommerse, J. P. M.; Stone, A. J.; Taylor, R.; Allen, F. H. *J. Am. Chem. Soc.* **1996**, *118*, 3108−3116.

(2) (a) Dumas, J. M.; Peurichard, H.; Gomel, M. *J. Chem. Res., Synop.* **1978**, 54−55. (b) Dumas, J. M., Gomel, M., Guérin, M. In *Molecular Interactions involving Organic Halides. The Chemistry of Functional Groups Supplement D*; Wiley: New York, 1983; pp 983−1020. (c) Legon, A. C. *Angew. Chem., Int. Ed.* **1999**, *38*, 2686−2714. (d) Legon, A. C. *Phys. Chem. Chem. Phys.* **2010**, *12*, 7736−7747.

(3) (a) Forni, A.; Metrangolo, P.; Pilati, T.; Resnati, G. *Cryst. Grow. Des.* **2004**, *4*, 291−295. (b) Desiraju, G. R., Ho, P. S., Kloo, L., Legon, A. C., Marquardt, R., Metrangolo, P., Politzer, P. A., Resnati, G., Rissanen, K. *Definition of the halogen bond* IUPAC Provisional Recommendation, http://www.iupac.org/home/publications/provisional-recommendations/under-review-by-the-authors/under-review-by-the-authors-container/definition-of-the-halogen-bond.html, http://www.halogenbonding.eu/ (accessed July 4, 2013).

(4) (a) Aakeröy, C. B.; Fasulo, M.; Schulteiss, N.; Desper, J.; Moore, C. *J. Am. Chem. Soc.* **2007**, *129*, 13772−13773. (b) Domagała, M.; Matczak, P.; Palusiak, M. *Comput. Theor. Chem.* **2012**, *998*, 26−33. (c) Metrangolo, P.; Neukirch, H.; Pilati, T.; Resnati, G. *Acc. Chem. Res.* **2005**, *38*, 386−395. (d) Politzer, P.; Murray, J. S.; Clark, T. *Phys. Chem. Chem. Phys.* **2010**, *12*, 7748−7757. (e) Troff, R. W.; Mäkelä, T.; Topić, F.; Valkonen, A.; Raatikainen, K.; Rissanen, K. *Eur. J. Org. Chem.* **2013**, *14*, 1617−1637. (f) Shin, K. S.; Brezgunova, M.; Jeannin, O.; Roisnel, T.; Auban-Senzier, C. P.; Fourmigué, M. *Cryst. Growth Des.* **2011**, *11*, 5337−5345.

(5) (a) Corradi, E.; Meille, S. V.; Messina, M. T.; Metrangolo, P.; Resnati, G. *Angew. Chem., Int. Ed.* **2000**, *39*, 1782−1786. (b) Auffinger, P.; Hays, F. A.; Westhof, E.; Ho, P. S. *Proc. Natl. Acad. Sci. U.S.A.* **2004**, *101*, 16789−16794. (c) Cinčić, D.; Friscic, T.; Jones, W. *Chem.—Eur. J.* **2008**, *14*, 747−753. (d) Cinčić, D.; Friscic, T.; Jones, W. *J. Am. Chem. Soc.* **2008**, *130*, 7524−7525. (d) Gavezzotti, A. *Mol. Phys.* **2008**, *106*, 1473−1485. (e) Fourmigué, M. *Curr. Opin. Solid State Mater. Sci.* **2009**, *13*, 36−45. (f) Shirman, T.; Arad, T.; van der Boom, M. E. *Angew. Chem., Int. Ed.* **2010**, *49*, 926−929. (g) Parisini, E.; Metrangolo, P.; Pilati, T.; Resnati, G.; Terraneo, G. *Chem. Soc. Rev.* **2011**, *40*, 2267−2279. (h) Lieffrig, J.; Jeannin, O.; Cuizouarn, T.; Auban-Senzier, P.; Fourmigué, M. *Cryst. Growth Des.* **2012**, *12*, 4248−4257.

(6) (a) Metrangolo, P.; Resnati, G. *Chem.—Eur. J.* **2001**, *7*, 2511−2519. (b) Metrangolo, P.; Resnati, G.; Pilati, T.; Liantonio, R.; Meyer, F. *J. Polym. Sci., Part A: Polym. Chem.* **2007**, *45*, 1−15. (c) Espallargas, G. M.; Zordan, F.; Marin, H. A.; Shankland, K.; van der Streek, J.; Brammer, L. *Chem.—Eur. J.* **2009**, *15*, 7554−7568. (d) Politzer, P.; Riley, K. E.; Bulat, F. A.; Murray, J. S. *Comput. Theor. Chem.* **2012**, *998*, 2−8. (e) Cauliez, P.; Polo, V.; Roisnel, T.; Llusar, R.; Fourmigué, M. *CrystEngComm* **2010**, *12*, 558−566.
(7) (a) Metrangolo, P.; Meyer, F.; Pilati, T.; Resnati, G.; Terraneo, G. *Angew. Chem., Int. Ed.* **2008**, *47*, 6114−6127. (b) Hathwar, V. R.; Guru Row, T. N. *J. Phys. Chem. A* **2010**, *114*, 13434−13441. (c) Hathwar, V. R.; Guru Row, T. N. *Cryst. Growth Des.* **2011**, *11*, 1338−1346. (d) Hathwar, V. R.; Gonnade, R. G.; Munshi, P.; Bhadhade, M. M.; Guru Row, T. N. *Cryst. Growth Des.* **2011**, *11*, 1855−1862. (e) Fourmigué, M.; Batail, P. *Chem. Rev.* **2004**, *104*, 5379−5418. (f) Palusiak, M., Bankiewicz, B. *Structural Chemistry* 2013, in press, 10.1007/s11224-012-0157-1.
(8) Palusiak, M. *J. Mol. Struct., THEOCHEM* **2010**, *945*, 89−92.
(9) Grabowski, S. J. *J. Phys. Chem. A* **2012**, *116*, 1838−1845.
(10) (a) Murray, J.S..; Lane, P.; Clark, T.; Politzer, P. *J. Mol. Model.* **2007**, *13*, 1033−1038. (b) Murray, J. S.; Riley, K. E.; Politzer, P.; Clark, T. *Aust. J. Chem.* **2010**, *63*, 1598−1607. (c) Politzer, P.; Riley, K. E.; Bulta, F. A.; Murray, J. S. *Comput. Theor. Chem.* **2012**, *998*, 2−8. (d) Riley, K. E.; Hobza, P. *J. Chem. Theory Comput.* **2008**, *4*, 232−242. (e) Triguero, S.; Llusar, R.; Polo, V.; Furmigue, M. *Cryst. Growth Des.* **2008**, *8*, 2241−2247.
(11) (a) Azov, V. A.; Zeller, M.; Watat, M. L.; Xin, Y. *J. Mol. Struct.* **2011**, *1004*, 296−302. (b) Vande Velde, C. M. L.; Zeller, M.; Azov, V. A. *J. Mol. Struct.* **2012**, *1016*, 109−117. (c) Bakavoli, M.; Rahimizadeh, M.; Feizyzadeh, B.; Kaju, A. A.; Takjoo, R. *J. Chem. Crystallogr.* **2010**, *40*, 746−752. (d) Fuller, R. O.; Griffith, C. S.; Koutsantonis, G. A.; Lapere, K. M.; Skelton, B. W.; Spackman, M. A.; White, A. H.; Wild, D. A. *CrystEngComm* **2012**, *14*, 804−811. (e) Wallentin, C. J.; Orentas, E.; Johnson, M. T.; Bathori, N. B.; Butkus, E.; Wendt, O. F.; Wärnmark, K.; Öhrström, L. *CrystEngComm* **2012**, *14*, 178−187. (f) Hathwar, V. R.; Gonnade, R. G.; Munshi, P.; Bhadbhade, M. M.; Guru Row, T. N. *Cryst. Growth Des.* **2011**, *11*, 1855−1862. (g) Hoser, A. A.; Dobrzycki, Ł.; Gutmann, M. J.; Woźniak, K. *Cryst. Growth Des.* **2010**, *10*, 5092−5104.
(12) Chęcińska, L.; Grabowsky, S.; Małecka, M.; Rybarczyk-Pirek, A. J.; Jóźwiak, A.; Paulmann, C.; Luger, P. *Acta Crystallogr., Sect. B* **2011**, *B67*, 133−144.
(13) Kabsch, W. *Acta Crystallogr., Sect. D* **2010**, *D66*, 569−581.
(14) *CrysAlis PRO*; Agilent Technologies: Yarnton, England, 2011.
(15) *XPREP*; Bruker AXS Inc.: Madison, Wisconsin, 2005.
(16) Sheldrick, G. M. *Acta Crystallogr., Sect. A* **2008**, *A64*, 112−122.
(17) Nardelli, M. *J. Appl. Crystallogr.* **1995**, *28*, 659−659.
(18) Spek, A. L. *J. Appl. Crystallogr.* **2003**, *36*, 7−13.
(19) Farrugia, L. J. *J. Appl. Crystallogr.* **1999**, *32*, 837−838.
(20) Frisch, M. J., Trucks, G. W., Schlegel, H. B., Scuseria, G. E., Robb, M. A., Cheeseman, J. R., Scalmani, G., Barone, V., Mennucci, B., Petersson, G. A., Nakatsuji, H., Caricato, M., Li, X., Hratchian, H. P., Izmaylov, A. F., Bloino, J., Zheng, G., Sonnenberg, J. L., Hada, M., Ehara, M., Toyota, K., Fukuda, R., Hasegawa, J., Ishida, M., Nakajima, T., Honda, Y., Kitao, O., Nakai, H., Vreven, T., Montgomery, J. A. Jr., Peralta, J. E., Ogliaro, F., Bearpark, M., Heyd, J. J., Brothers, E., Kudin, K. N., Staroverov, V. N., Kobayashi, R., Normand, J., Raghavachari, K., Rendell, A., Burant, J. C., Iyengar, S. S., Tomasi, J., Cossi, M., Rega, N., Millam, J. M., Klene, M., Knox, J. E., Cross, J. B., Bakken, V., Adamo, C., Jaramillo, J., Gomperts, R., Stratmann, R. E., Yazyev, O., Austin, A. J., Cammi, R., Pomelli, C., Ochterski, J. W., Martin, R. L., Morokuma, K., Zakrzewski, V. G., Voth, G. A., Salvador, P., Dannenberg, J. J., Dapprich, S., Daniels, A. D., Farkas, Ö., Foresman, J. B., Ortiz, J. V., Cioslowski, J., Fox, D. J. *Gaussian 09*, revision A.1; Gaussian, Inc.: Wallingford CT, 2009.
(21) (a) Spackman, M. A.; McKinnon. *CrystEngComm* **2002**, *4*, 378−392. (b) Spackman, M.; Jayatilaka, D. *CrystEngComm* **2009**, *11*, 19−32. (c) Spackman, M. A.; McKinnon, J. J.; Jayatilaka, D. *CrystEngComm* **2008**, *10*, 377−388.
(22) Allen, F. H.; Kennard, O.; Watson, D. G.; Brammer, L.; Orpen, A. G.; Taylor, R. *J. Chem. Soc., Perkin Trans. 2* **1987**, S1−S19.
(23) Rybarczyk-Pirek, A. J. *Struct. Chem.* **2012**, *23*, 1739−1749.
(24) Etter, M. C.; MacDonald, J. C.; Bernstein, J. *Acta Crystallogr., Sect. B* **1990**, *B46*, 256−62.
(25) Bondi, A. *J. Phys. Chem.* **1964**, *68*, 441−451.
(26) Bilewicz, E.; Rybarczyk-Pirek, A. J.; Dubis, A. T.; Grabowski, S. J. *J. Mol. Struct.* **2007**, *829*, 208−211.
(27) (a) Zordan, F.; Brammer, L.; Sherwood, P. *J. Am. Chem. Soc.* **2005**, *127*, 5979−5989. (b) Awwadi, F. F.; Willet, R. D.; Peterson, K. A.; Twamley, B. *Chem.—Eur. J.* **2006**, *12*, 8952−8960. (c) Reddy, M. C.; Kirchner, M. T.; Gundakaram, R. C.; Padmanabham, K. A.; Desiraju, G. R. *Chem.—Eur. J.* **2006**, *12*, 2222−2234. (d) Thanh Thu Bui, T.; Dahaoui, S.; Lecomte, C.; Desiraju, G. R.; Espinosa, E. *Angew. Chem., Int. Ed.* **2009**, *48*, 3838−3842. (e) Brammer, L.; Espallargas, G. M.; Libri, S. *CrystEngComm* **2008**, *10*, 1712−1727. (f) Mukhejree, A.; Desiraju, G. R. *Cryst. Grow. Des.* **2011**, *11*, 3735−3739.
(28) (a) Adams, H.; Cockroft, S. L.; Guardigli, C.; Hunter, C. A.; Lawson, K. R.; Perkins, J.; Spey, E. S.; Urch, J. U.; Ford, R. *ChemBiolChem* **2004**, *5*, 657−665. (b) Swierczynski, D.; Luboradzki, R.; Dolgonos, G.; Lipkowski, J.; Schneider, H. J. *Eur. J. Org. Chem.* **2005**, 1171−1177. (c) Lu, Y. X.; Zou, J. W.; Wang, Y. H.; Yu, Q. S. *Chem. Phys.* **2006**, *334*, 1−7. (d) Fuller, O. R.; Griffith, C. S.; Koutsantonis, G. A.; Lapere, K. M.; Skelton, B. W.; Spackman, M. A.; White, A. H.; Wild, D. A. *CrystEngComm* **2012**, *14*, 804−811.
(29) Allen, F. H. *Acta Crystallogr., Sect. B* **2002**, *B58*, 380−388.
(30) (a) McKinnon, J. J.; Spackman, M. A.; Mitchell, A. S. *Acta Crystallogr., Sect. B* **2004**, *B60*, 627−668. (b) McKinnon, J. J.; Fabbiani, F. P. A.; Spackman, M. A. *Cryst. Growth Des.* **2007**, *7*, 755−769.